PBPK for Ritonavir booster

A minimal whole-body PBPK model to inform treatment adjustment with ritonavir (100mg, b.i.d.) introduced into a regimen

Andreas D. Meid

29 6 2022

Table of Contents

1 Background and rationale

This is an accompanying document to https://ritonavir-booster.shinyapps.io/Midazolam/ and the respective original publication submitted to *Journal*.

The motivation and rationale come from the Covid19 drug *Paxlovid(R)* introduced onto the market, which contains ritonavir (RTV), a protease inhibitor for so-called boosting (*Heskin et al. 2022*). Ritonavir is considered a potent perpetrator compound (*Polasek et al. 2011*), for which a variety of interactions mediated via the CYP3A4 system have been described (*Ernest et al. 2005*). Management of these interactions is exceedingly important when ritonavir is introduced into ongoing treatment (*Mikus et al. 2022*, *Guy-Alfandary et al. 2022*, *Marzolini et al. 2022*). Recently, specific adjustments in the treatment schedule of oral anticoagulants (*Wang & Chan 2022*) and cystic fibrosis therapeutics (*Hong et al. 2022*) based on physiology-based pharmacokinetics (PBPK) models have been developed.

The aim of this project is therefore to develop a PBPK platform that can be used to extrapolate the extent of a drug-drug interaction (DDI) to any substance and to make model-informed decisions to adjust treatment. To this end, a minimal PBPK model will be developed based on common input parameters that can then be adjusted depending on the substance. The model will be verified against existing evidence and real-world data.

2 Course of action

2.1 Figure 1: Course of working steps for the development of the PBPK model

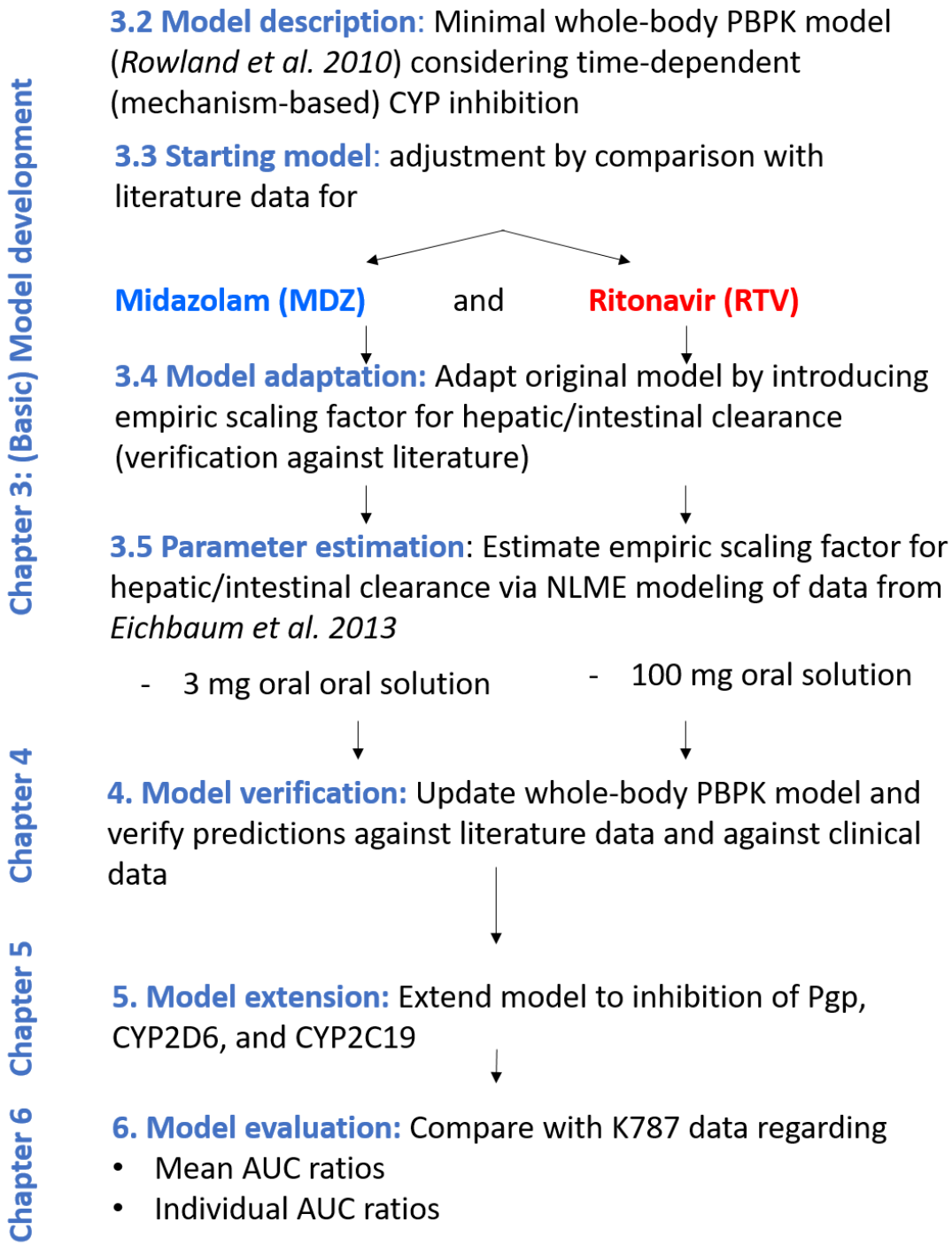

Legend:

3 Basic minimal whole-body PBPK model

A structural model was adapted from *Rowland et al. 2010*. Drug distribution is given by inter-connectivity of anatomy in mass balance equations, with the following simplifications:

- "well-stirred" distribution in liver and intestinal wall (Q_{gut}-model)
- unsegmented instestinal absorption
- first-order absorption process
- liver and kidney as elimination organs
- unbound (blood) concentration (fully) available for enzymatic Reactions.

The structural model was further extended to consider also time-dependent (mechanism-based) inhibition of CYP enzymes.

3.1 Figure 2: Structural model

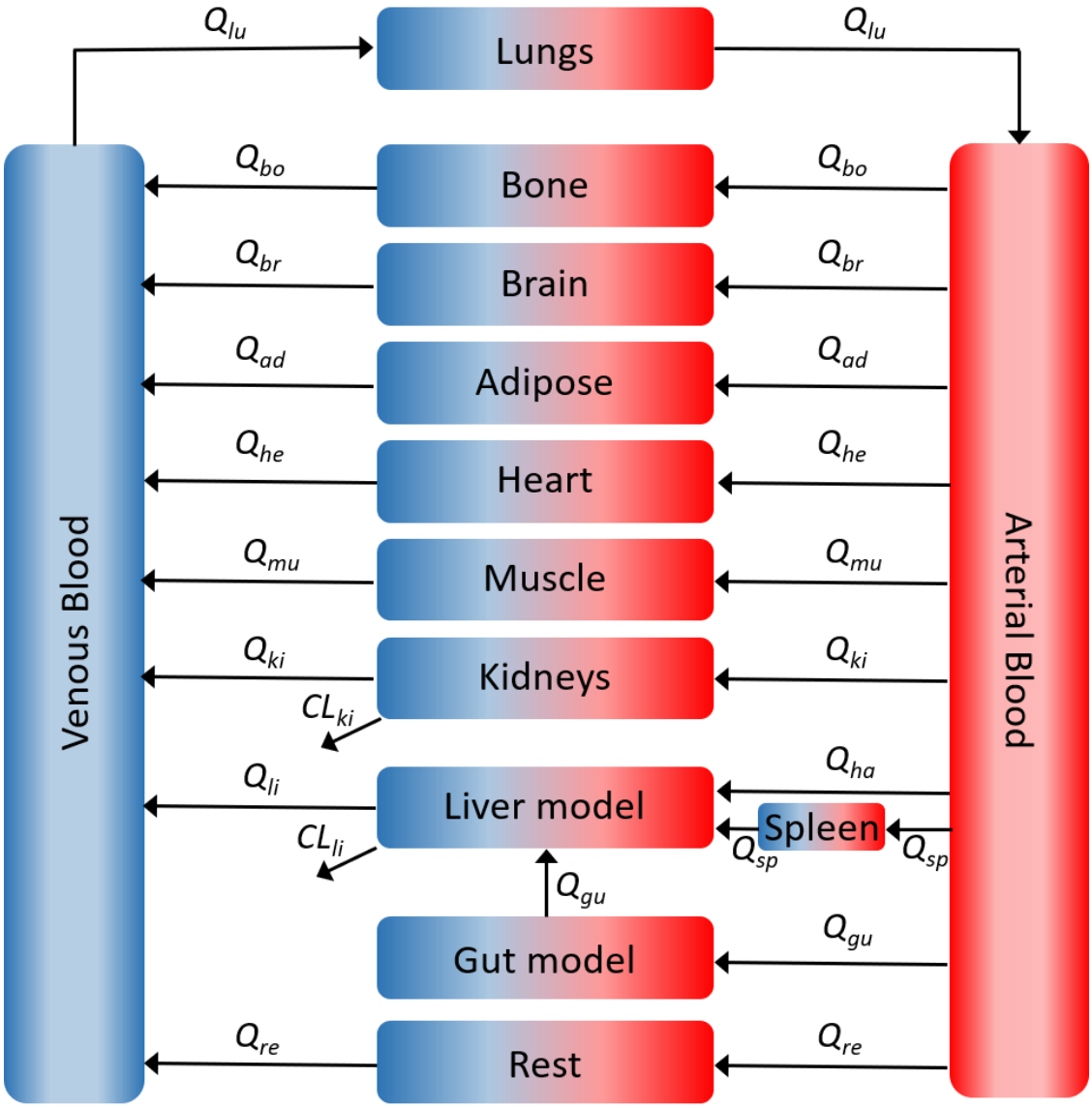

3.2 Model description

3.2.1 Absorption

The absorption model according to *Zane & Thakker 2014* was applied.

3.2.2 Distribution

Distribution in organs (compartments) without elimination is described by the following equation:

$$V_T \times \mathrm{d}C_t/\mathrm{d}t = Q_T \times C_A - Q_T \times Cv_T$$

with Q = blood flow (L/h), C = concentration (mg/L), V = volume (L), T = organ/tissue, A = arterial, V = venous, and

$$Cv_T = \frac{C_t}{Kp/B{:}P}$$

with substance-specific partition coefficients *Kp* estimated according to *Poulin & Theil 2002* and *B:P* as the blood-plasma partition coefficient.

3.2.3 Metabolism

The *in vitro - in vivo* - extrapolated enzymatic clearance (apparent, (*app*)) is:

$$CL_{int,(app)}(t) = \frac{Vmax \cdot Enz(t)}{K_m + f_u \cdot C}$$

with f_u as free unbound fraction, V_{max} as maximum metabolic reaction rate according to Michaelis-Menten together with the corresponding constant K_m (corrected for non-specific binding), and *Enz(t)* as active enzyme abundance. It is scaled up with *MPPGL* corresponding to milligrams of microsomal protein per gram of liver (mg/g) (estimated according to *Barter et al. 2008*), *LW* as liver weight (kg), $f_{u,inc}$ as the fraction unbound in the *in vitro* system according to:

$$CL_{int,scaled} = \frac{CL_{int,app}}{f_{u,inc}} \times MPPGL \times LW$$

Dynamically, mechanism-based inhibition of CYP enzymes takes into account temporal enzyme abundance:

$$\frac{dE_t}{dt} = k_{deg} \times (E_{Baseline} - E_t) - \left(\frac{k_{inact} \times TDI}{K_I} \times E_t\right)$$

with k_{deg} as the first-order rate constant of enzyme degradation, which when multiplied by the net abundance at time t ($E_{baseline} - E_t$) corresponds to the rate of synthesis of the enzyme under equilibrium conditions. The last term is the rate of elimination from the enzyme pool, which depends on the maximum first-order inactivation rate (k_{inact}), the unbound concentration of the time-dependent inhibitor (*TDI*), and the apparent

dissociation constant K_I (between enzyme and inhibitor). The intrinsic clearance CL_{int} (mL/min) is thus given by the multiplication

$$CL_{int}(mL/min) = \frac{CL_{int}\left(mL/min/pmol_{Enzym-Isoform}\right) \times E_t}{1}$$

3.2.4 Elimination

For mass balance with elimination, the following applies (after *Jones and Rowland-Yeo 2013*):

$$V_T \times \mathrm{d}C_t/\mathrm{d}t = Q_T \times C_A - Q_T \times Cv_T - CL_{int} \times Cv_{uT}$$

, where renal elimination depends on renal clearance (CL_{renal}) and hepatic elimination occurs with the (intrinsic) clearance as derived above.

3.3 Starting model

Initially, the model was developed on the basis of comparisons with the literature (see section 4 for a conclusion), using the parameters given in **Table 1** at the beginning. For comparisons with the literature, a lag time for ritonavir was additionally considered (Kappelhoff et al. 2005).

3.3.1 Table 1: Model parameters of PBPK starting model

descr	unit	options	value
body weight	kg	standard	73
age	years	standard	40
empiric scaling of CYP3A5 clearance	factor	dummy	1
empiric scaling of intestinal CYP clearance	factor	dummy	1
empiric scaling of hepatic CYP clearance	factor	dummy	1
Adipose tissue volume	L	ICRP 2002	18.2
Adipose fraction of tissue blood flow	.	ICRP 2002	0.05
Bone tissue volume	L	ICRP 2002	10.5
Bone fraction of tissue blood flow	.	ICRP 2002	0.05
Brain tissue volume	L	ICRP 2002	1.45
Brain fraction of tissue blood flow	.	ICRP 2002	0.12
Gut (wall) tissue volume	L	ICRP 2002	0.65
Gut fraction of tissue blood flow	wall	ICRP 2002	0.15
Gut (lumen) tissue volume	L	ICRP 2002	0.35
Heart tissue volume	L	ICRP 2002	0.33
Heart fraction of tissue blood flow	.	ICRP 2002	0.04

descr	unit	options	value
Kidney tissue volume	L	ICRP 2002	0.31
Kidney fraction of tissue blood flow	.	ICRP 2002	0.19
Liver tissue volume	L	ICRP 2002	1.8
Liver fraction of tissue blood flow	.	ICRP 2002	0.255
Lung tissue volume	L	ICRP 2002	0.5
Lung fraction of tissue blood flow	same as cardiac output	ICRP 2002	1
Muscle tissue volume	L	ICRP 2002	29
Muscle fraction of tissue blood flow	.	ICRP 2002	0.17
Spleen tissue volume	L	ICRP 2002	0.15
Spleen fraction of tissue blood flow	.	ICRP 2002	0.03
(Arterial) blood tissue volume	L	ICRP 2002	5.6
Hepatic artery fraction of tissue blood flow	.	ICRP 2002	0.065
Cardiac output	L/min	ICRP 2002	6.5
hepatic CYP3A4 enzyme abundance	pmol/mg	Zanger et al. 2013	93
hepatic CYP3A4 enzyme abundance	pmol/mg	Wang et al. 2016	82
hepatic CYP2D6 enzyme abundance	pmol/mg	.	12.6
hepatic CYP2C19 enzyme abundance	pmol/mg	.	11
intestinal CYP3A4 enzyme abundance	pmol/mg	Wang et al. 2016	58
intestinal CYP3A5 enzyme abundance	pmol/mg	Wang et al. 2016	21.5
degradation rate of CYP3A4	1/h	Rowland-Yeo et al. 2011	0.0193
degradation rate of CYP3A5	1/h	Rowland-Yeo et al. 2011	0.0193
degradation rate of CYP2C19	1/h	Rowland-Yeo et al. 2011	0.0267
degradation rate of CYP2D6	1/h	Rowland-Yeo et al. 2011	0.0143
Adipose:plasma partition coefficient of Ritonavir	.	Poulin & Theil 2002	2.315

descr	unit	options	value
Adipose:plasma partition coefficient of Midazolam	.	Poulin & Theil 2002	2.26
Bone:plasma partition coefficient of Ritonavir	.	Poulin & Theil 2002	2.315
Bone:plasma partition coefficient of Midazolam	.	Poulin & Theil 2002	8.79
Brain:plasma partition coefficient of Ritonavir	.	Poulin & Theil 2002	8.791
Brain:plasma partition coefficient of Midazolam	.	Poulin & Theil 2002	8.04
Gut:plasma partition coefficient of Ritonavir	.	Poulin & Theil 2002	8.043
Gut:plasma partition coefficient of Midazolam	.	Poulin & Theil 2002	6.34
Heart:plasma partition coefficient of Ritonavir	.	Poulin & Theil 2002	6.344
Heart:plasma partition coefficient of Midazolam	.	Poulin & Theil 2002	1.96
Kidney:plasma partition coefficient of Ritonavir	.	Poulin & Theil 2002	1.959
Kidney:plasma partition coefficient of Midazolam	.	Poulin & Theil 2002	3.03
Liver:plasma partition coefficient of Ritonavir	.	Poulin & Theil 2002	3.033
Liver:plasma partition coefficient of Midazolam	.	Poulin & Theil 2002	5.02
Lungs:plasma partition coefficient of Ritonavir	.	Poulin & Theil 2002	5.018
Lungs:plasma partition coefficient of Midazolam	.	Poulin & Theil 2002	0.686
Muscle:plasma partition coefficient of Ritonavir	.	Poulin & Theil 2002	0.6858
Muscle:plasma partition coefficient of Midazolam	.	Poulin & Theil 2002	3.08
Spleen:plasma partition coefficient of Ritonavir	.	Poulin & Theil 2002	3.079
Spleen:plasma partition coefficient of Midazolam	.	Poulin & Theil 2002	3.09
Rest:plasma partition coefficient of Ritonavir	.	Poulin & Theil 2002	3.761

descr	unit	options	value
Rest:plasma partition coefficient of Midazolam	.	Poulin & Theil 2002	4.467
blood:plasma ratio of Ritonavir	.	Siccardi et al. 2013, Molto et al. 2016	0.587
blood:plasma ratio of Midazolam	.	Rowland-Yeo et al. 2011	0.603
Ritonavir absorption rate constant	/hr	.	0.22
Ritonavir bioavailability	.	.	0.93
Ritonavir fraction available for absorption from dosage form	.	Rowland-Yeo et al. 2011	0.96
Ritonavir gut availability	.	Rowland-Yeo et al. 2011	1
Ritonavir fraction of unbound drug in plasma	.	Siccardi et al. 2013, Hsu et al. 1997	0.015
Ritonavir fraction of unbound drug in the in vitro hepatocyte incubation	.	Drewe et al. 1999, Colbers et al 2016	0.233
Ritonavir plasma-to-whole-liver concentration ratio	.	Choi et al. 2019	13.3
Midazolam absorption rate constant	/hr	Rowland-Yeo et al. 2011	3.04
Midazolam bioavailability	.	.	0.93
Midazolam fraction available for absorption from dosage form	.	Utsey et al. 2020	0.88
Midazolam gut availability	.	Yang et al. 2007	0.59
Midazolam fraction of unbound drug in plasma	.	Rowland-Yeo et al. 2011	0.032
Ritonavir molecular weight [https	g/mol	.	720.9
Ritonavir log10 octanol oil:water partition coefficient [https	.	.	3.6
Midazolam molecular weight [https	g/mol	.	325.8
Midazolam log10 octanol oil:water partition coefficient [https	.	.	4.33
Ritonavir (intestinal lumen solubility) [https	mg/L	.	1.26
Midazolam (intestinal lumen solubility) [https	mg/L	.	9.87
small intestine length	cm	ICRP 2002	280
diameter of small intestine lumen	cm	ICRP 2002	2.5

descr	unit	options	value
plicae circulare factor	.	Helander & Fandriks 2014	1.57
villi factor	.	Helander & Fandriks 2014	6.5
microvilli factor	.	Helander & Fandriks 2014	13
small intestine transit time	h	Olivares-Morales et al. 2015	3.32
constant in the permeability calculation equation https	.	Willmann et al. 2004	7440
constant in the permeability calculation equation	.	Willmann et al. 2004	10000000
constant in the permeability calculation equation	.	Willmann et al. 2004	0.6
constant in the permeability calculation equation	.	Willmann et al. 2004	4.395
absorption factor to manipulate ka	.	Willmann et al. 2004	1
disappearance from gut lumen factor to manipulate kd	.	Willmann et al. 2004	1
permeability factor to manipulate Pm	.	Willmann et al. 2004	1
Ritonavir fraction of unbound drug in microsomes	.	Rowland Yeo et al. 2010	0.71
Ritonavir CYP3A4 adult hepatic Vmax	pmol/min/pmol CYP	Koudriakova et al. 1998	1.37
Ritonavir CYP3A4 adult hepatic Km	uM	Koudriakova et al. 1998	0.07
Ritonavir CYP3A5 adult hepatic Vmax	pmol/min/pmol CYP	Koudriakova et al. 1998	1
Ritonavir CYP3A5 adult hepatic Km	uM	Koudriakova et al. 1998	0.05
Ritonavir CYP2D6 adult hepatic Vmax	pmol/min/pmol CYP	Koudriakova et al. 1998	1
Ritonavir CYP2D6 adult hepatic Km	uM	Koudriakova et al. 1998	0.7
Midazolam fraction of unbound drug in microsomes	.	Rowland Yeo et al. 2010	1
Midazolam CYP3A4 adult hepatic Vmax	pmol/min/pmol CYP	Simcyp default	5.23
Midazolam CYP3A4 adult hepatic	uM	Simcyp default	2.16

descr	unit	options	value
Km			
Midazolam CYP3A5 adult hepatic Vmax	pmol/min/pmol CYP	Simcyp default	19.7
Midazolam CYP3A5 adult hepatic Km	uM	Simcyp default	4.16
Ritonavir renal clearance	L/hr	Molto et al. 2016	0.53
Midazolam renal clearance	L/hr	Rowland-Yeo et al. 2011	0.085
CYP3A4 competitive inhibition constant	mM	Colbers et al. 2016	0.02928
CYP2D6 competitive inhibition constant	mM	Colbers et al. 2016	2.9
Mechanism-based CYP3A4 maximum inactivation rate constant	1/h	Kaspera et al. 2014	192
Mechanism-based CYP3A4 apparent enzyme inhibition constant	.	Kaspera et al. 2014	0.091
Mechanism-based CYP3A5 maximum inactivation rate constant	1/h	Kaspera et al. 2014	40
Mechanism-based CYP3A5 apparent enzyme inhibition constant	.	Kaspera et al. 2014	0.1092
Lag-time Ritonavir administration	h	Kappelhoff et al. 2005	0.778

3.4 Model updating

The starting model was updated with the following aspects:

- the RTV absorption constant (*ka*) was chosen according to *Hsu et al. 1997*
- the (smaller and variable) influence of CYP3A5 (relative to CYP3A4) was multiplied by a factor of 0.118 following inter-system extrapolation factors (ISEFs, *Umehara et al. 2017*)
- additional scaling factors were introduced for flow-dependent intestinal and hepatic clearance and enzymatic intestinal and hepatic clearance capacity (*skala_gut_clearance*, *skala_liver_clearance*, *skala_gut_enzyme*, *skala_liver_enzyme*)

3.5 Estimation of empiric scaling factor for hepatic/intestinal clearance via NLME modeling of data from *Eichbaum et al. 2013*

The scaling factors for flow-dependent intestinal and hepatic clearance and enzymatic intestinal and hepatic clearance capacity (*skala_gut_clearance*, *skala_liver_clearance*, *skala_gut_enzyme*, *skala_liver_enzyme*) were initially chosen manually in order to achieve a good agreement of the model predictions with the concentration-time profiles from the literature. With original data from the study by *Eichbaum et al. 2013* at hand, the updated PBPK model was used for parameter estimation using nonlinear mixed-effects modeling (NLME).

3.5.1 MDZ

For the MDZ part, the scaling factor for hepatic clearance was estimated including inter-intervidual variability (fixed effect plus random effect), whereas the flow-dependent scaling factors for hepatic and intestinal clearance were estimated for the population mean alone (fixed effects). **Figure 5** shows the fitted individual profiles.

3.5.2 RTV

For the RTV part, convergence could not be technically achieved if the scaling parameters were to be estimated in the PBPK model using NLME. Alternatively, a one-compartment model with inter-individual variability in clearance and volume of distribution was fitted to the data in order to compare the PBPK model with individual fits. **Figure 5** shows the fitted individual profiles.

4 Verification of updated PBPK model

Verification was performed using concentration-time profiles from the literature. Model predictions were either superimposed on the adopted original images or plotted with the literature's mean concentrations being extracted by using WebPlotDigitizer (https://automeris.io/WebPlotDigitizer/). Both measured values and PBPK model predictions were considered. Finally, the updated PBPK was also compared to the data of *Eichbaum et al. 2013*.

4.1 Figure 3: MDZ comparison with the literature

- clinical data and PBPK model predictions

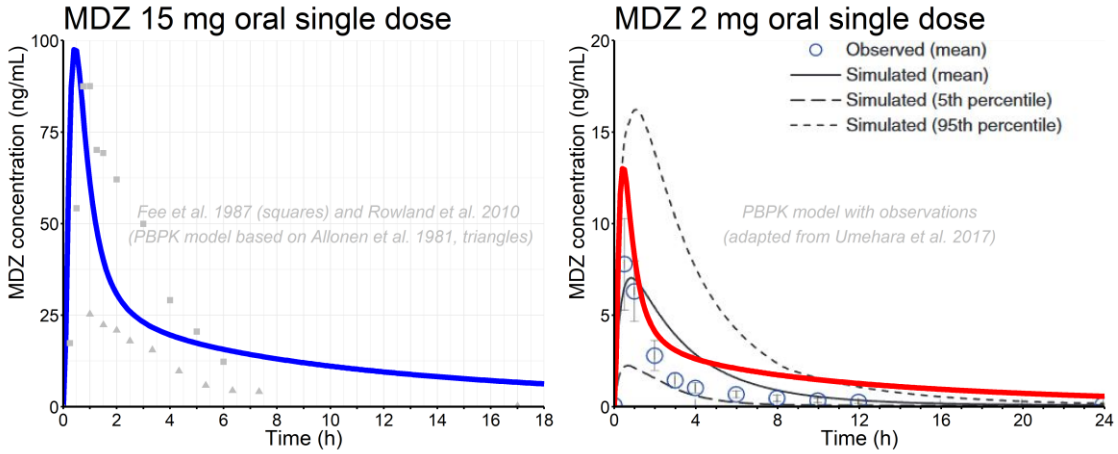

4.2 Figure 4: RTV comparison with the literature

- A: clinical data

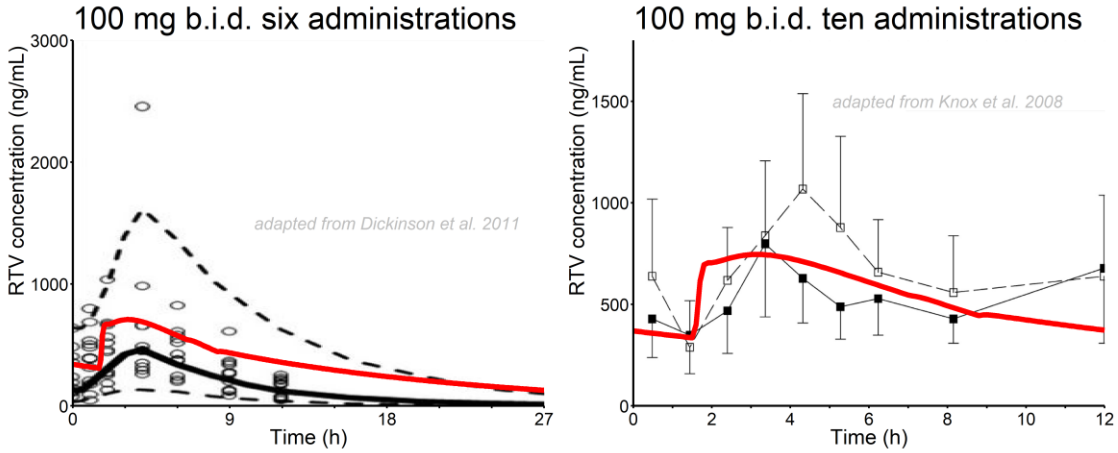

- B: PBPK model predictions

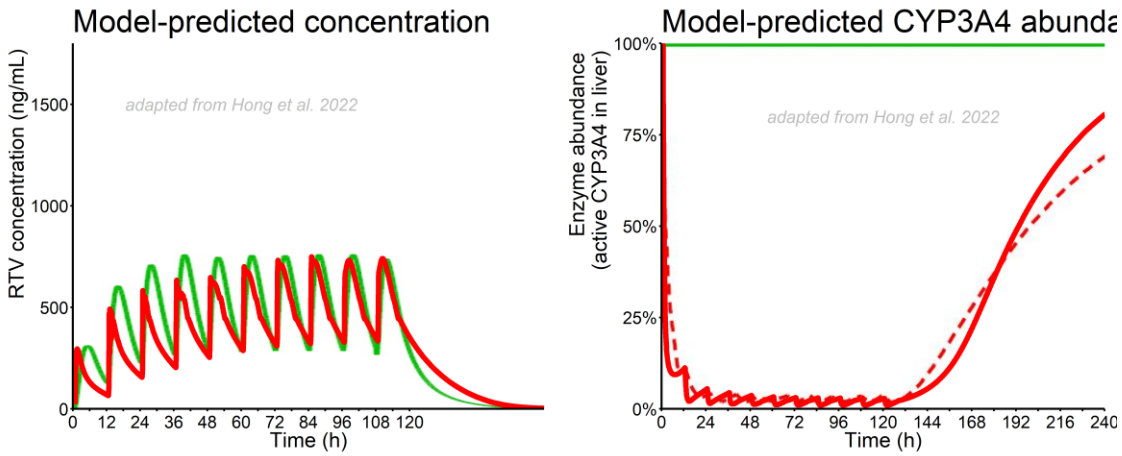

4.3 Figure 5: MDZ and RTV empirically compared with individual fits

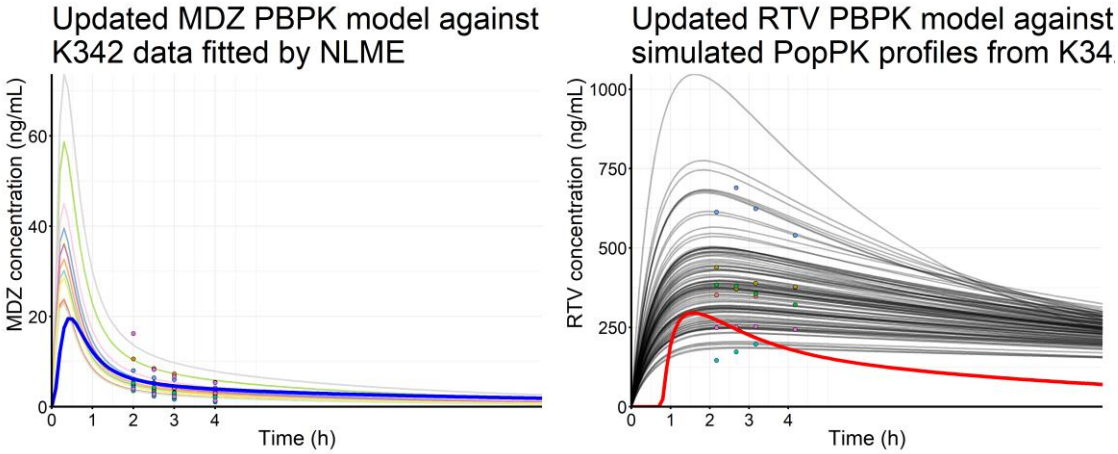

5 Model extension for inhibition of Pgp, CYP2D6, and CYP2C19

5.1 Figure 6: Efflux transport

6 Model evaluation with current study data (K787)

7 Outlook

8 References

- Barter, Z. E., J. E. Chowdry, J. R. Harlow, J. E. Snawder, J. C. Lipscomb and A. Rostami-Hodjegan (2008). Covariation of human microsomal protein per gram of liver with age: absence of influence of operator and sample storage may justify interlaboratory data pooling. Drug Metab Dispos 36(12): 2405-2409.
- Choi, G. W., Y. B. Lee and H. Y. Cho (2019). Interpretation of Non-Clinical Data for Prediction of Human Pharmacokinetic Parameters: In Vitro-In Vivo Extrapolation and Allometric Scaling. Pharmaceutics 11(4).
- Colbers, A., R. Greupink, C. Litjens, D. Burger and F. G. Russel (2016). Physiologically Based Modelling of Darunavir/Ritonavir Pharmacokinetics During Pregnancy. Clin Pharmacokinet 55(3): 381-396.
- Custodio, J. M., K. M. Donaldson and H. J. Hunt (2021). An In Vitro and In Vivo Evaluation of the Effect of Relacorilant on the Activity of Cytochrome P450 Drug Metabolizing Enzymes. J Clin Pharmacol 61(2): 244-253.
- Dickinson, L., M. Boffito, D. Back, L. Else, N. von Hentig, G. Davies, S. Khoo, A. Pozniak, G. Moyle and L. Aarons (2011). Sequential population pharmacokinetic modeling of lopinavir and ritonavir in healthy volunteers and assessment of different dosing strategies. Antimicrob Agents Chemother 55(6): 2775-2782.
- Drewe, J., H. Gutmann, G. Fricker, M. Torok, C. Beglinger and J. Huwyler (1999). HIV protease inhibitor ritonavir: a more potent inhibitor of P-glycoprotein than the cyclosporine analog SDZ PSC 833. Biochem Pharmacol 57(10): 1147-1152.
- Eichbaum, C., M. Cortese, A. Blank, J. Burhenne and G. Mikus (2013). Concentration effect relationship of CYP3A inhibition by ritonavir in humans. Eur J Clin Pharmacol 69(10): 1795-1800.
- Ernest, C. S., 2nd, S. D. Hall and D. R. Jones (2005). Mechanism-based inactivation of CYP3A by HIV protease inhibitors. J Pharmacol Exp Ther 312(2): 583-591.
- Fee, J. P., P. S. Collier, P. J. Howard and J. W. Dundee (1987). Cimetidine and ranitidine increase midazolam bioavailability. Clin Pharmacol Ther 41(1): 80-84.
- Greenblatt, D. J., D. E. Peters, L. E. Oleson, J. S. Harmatz, M. W. MacNab, N. Berkowitz, M. A. Zinny and M. H. Court (2009). Inhibition of oral midazolam clearance by boosting doses of ritonavir, and by 4,4-dimethyl-benziso-(2H)-selenazine (ALT-2074), an experimental catalytic mimic of glutathione oxidase. Br J Clin Pharmacol 68(6): 920-927.
- Guy-Alfandary, S., S. Zhurat, M. Berlin, T. De Haan, I. Gueta, R. Shihmanter, A. Golik, M. Berkovitch, S. Eyal and L. H. Goldstein (2022). Managing Potential Drug Interactions of Nirmatrelvir/Ritonavir in COVID-19 Patients: A Perspective from an Israeli Cross-Sector Collaboration. Clin Pharmacol Ther.
- Helander, H. F. and L. Fandriks (2014). Surface area of the digestive tract - revisited. Scand J Gastroenterol 49(6): 681-689.
- Heskin, J., S. J. C. Pallett, N. Mughal, G. W. Davies, L. S. P. Moore, M. Rayment and R. Jones (2022). Caution required with use of ritonavir-boosted PF-07321332 in COVID-19 management. Lancet 399(10319): 21-22.
- Hong, E., L. M. Almond, P. S. Chung, A. P. Rao and P. M. Beringer (2022). Physiologically-Based Pharmacokinetic-Led Guidance for Patients With Cystic

Fibrosis Taking Elexacaftor-Tezacaftor-Ivacaftor With Nirmatrelvir-Ritonavir for the Treatment of COVID-19. Clin Pharmacol Ther.

- Hsu, A., G. R. Granneman, G. Witt, C. Locke, J. Denissen, A. Molla, J. Valdes, J. Smith, K. Erdman, N. Lyons, P. Niu, J. P. Decourt, J. B. Fourtillan, J. Girault and J. M. Leonard (1997). Multiple-dose pharmacokinetics of ritonavir in human immunodeficiency virus-infected subjects. Antimicrob Agents Chemother 41(5): 898-905.
- ICRP (2002). Basic anatomical and physiological data for use in radiological protection: reference values. A report of age- and gender-related differences in the anatomical and physiological characteristics of reference individuals. ICRP Publication 89. Ann ICRP 32(3-4): 5-265.
- Jones, H. and K. Rowland-Yeo (2013). Basic concepts in physiologically based pharmacokinetic modeling in drug discovery and development. CPT Pharmacometrics Syst Pharmacol 2: e63.
- Kappelhoff, B. S., A. D. Huitema, K. M. Crommentuyn, J. W. Mulder, P. L. Meenhorst, E. C. van Gorp, A. T. Mairuhu and J. H. Beijnen (2005). Development and validation of a population pharmacokinetic model for ritonavir used as a booster or as an antiviral agent in HIV-1-infected patients. Br J Clin Pharmacol 59(2): 174-182.
- Kaspera, R., B. J. Kirby, T. Sahele, A. C. Collier, E. D. Kharasch, J. D. Unadkat and R. A. Totah (2014). Investigating the contribution of CYP2J2 to ritonavir metabolism in vitro and in vivo. Biochem Pharmacol 91(1): 109-118.
- Kirby, B. J., A. C. Collier, E. D. Kharasch, D. Whittington, K. E. Thummel and J. D. Unadkat (2011). Complex drug interactions of HIV protease inhibitors 1: inactivation, induction, and inhibition of cytochrome P450 3A by ritonavir or nelfinavir. Drug Metab Dispos 39(6): 1070-1078.
- Knox, T. A., L. Oleson, L. L. von Moltke, R. C. Kaufman, C. A. Wanke and D. J. Greenblatt (2008). Ritonavir greatly impairs CYP3A activity in HIV infection with chronic viral hepatitis. J Acquir Immune Defic Syndr 49(4): 358-368.
- Koudriakova, T., E. Iatsimirskaia, I. Utkin, E. Gangl, P. Vouros, E. Storozhuk, D. Orza, J. Marinina and N. Gerber (1998). Metabolism of the human immunodeficiency virus protease inhibitors indinavir and ritonavir by human intestinal microsomes and expressed cytochrome P4503A4/3A5: mechanism-based inactivation of cytochrome P4503A by ritonavir. Drug Metab Dispos 26(6): 552-561.
- Marzolini, C., D. R. Kuritzkes, F. Marra, A. Boyle, S. Gibbons, C. Flexner, A. Pozniak, M. Boffito, L. Waters, D. Burger, D. J. Back and S. Khoo (2022). Recommendations for the Management of Drug-Drug Interactions Between the COVID-19 Antiviral Nirmatrelvir/Ritonavir (Paxlovid) and Comedications. Clin Pharmacol Ther.
- Mathias, A. A., S. West, J. Hui and B. P. Kearney (2009). Dose-response of ritonavir on hepatic CYP3A activity and elvitegravir oral exposure. Clin Pharmacol Ther 85(1): 64-70.
- Mikus, G., K. I. Foerster, T. Terstegen, C. Vogt, A. Said, M. Schulz and W. E. Haefeli (2022). Oral Drugs Against COVID-19-Management of Drug Interactions With the Use of Nirmatrelvir/Ritonavir. Dtsch Arztebl Int(Forthcoming).
- Molto, J., J. A. Estevez, C. Miranda, S. Cedeno, B. Clotet and M. Valle (2016). Population pharmacokinetic modelling of the changes in atazanavir plasma clearance caused by

ritonavir plasma concentrations in HIV-1 infected patients. Br J Clin Pharmacol 82(6): 1528-1538.
- Olivares-Morales, A., H. Lennernas, L. Aarons and A. Rostami-Hodjegan (2015). Translating Human Effective Jejunal Intestinal Permeability to Surface-Dependent Intrinsic Permeability: a Pragmatic Method for a More Mechanistic Prediction of Regional Oral Drug Absorption. AAPS J 17(5): 1177-1192.
- Pan, X., S. Yamazaki, S. Neuhoff, M. Zhang and V. Pilla Reddy (2021). Unraveling pleiotropic effects of rifampicin by using physiologically based pharmacokinetic modeling: Assessing the induction magnitude of P-glycoprotein-cytochrome P450 3A4 dual substrates. CPT Pharmacometrics Syst Pharmacol 10(12): 1485-1496.
- Polasek, T. M., F. P. Lin, J. O. Miners and M. P. Doogue (2011). Perpetrators of pharmacokinetic drug-drug interactions arising from altered cytochrome P450 activity: a criteria-based assessment. Br J Clin Pharmacol 71(5): 727-736.
- Poulin, P. and F. P. Theil (2002). Prediction of pharmacokinetics prior to in vivo studies. 1. Mechanism-based prediction of volume of distribution. J Pharm Sci 91(1): 129-156.
- Rowland Yeo, K., M. Jamei, J. Yang, G. T. Tucker and A. Rostami-Hodjegan (2010). Physiologically based mechanistic modelling to predict complex drug-drug interactions involving simultaneous competitive and time-dependent enzyme inhibition by parent compound and its metabolite in both liver and gut - the effect of diltiazem on the time-course of exposure to triazolam. Eur J Pharm Sci 39(5): 298-309.
- Rowland Yeo, K., R. L. Walsky, M. Jamei, A. Rostami-Hodjegan and G. T. Tucker (2011). Prediction of time-dependent CYP3A4 drug-drug interactions by physiologically based pharmacokinetic modelling: impact of inactivation parameters and enzyme turnover. Eur J Pharm Sci 43(3): 160-173.
- Siccardi, M., C. Marzolini, K. Seden, L. Almond, A. Kirov, S. Khoo, A. Owen and D. Back (2013). Prediction of drug-drug interactions between various antidepressants and efavirenz or boosted protease inhibitors using a physiologically based pharmacokinetic modelling approach. Clin Pharmacokinet 52(7): 583-592.
- Utsey, K., M. S. Gastonguay, S. Russell, R. Freling, M. M. Riggs and A. Elmokadem (2020). Quantification of the Impact of Partition Coefficient Prediction Methods on Physiologically Based Pharmacokinetic Model Output Using a Standardized Tissue Composition. Drug Metab Dispos 48(10): 903-916.
- Wang, H. Y., X. Chen, J. Jiang, J. Shi and P. Hu (2016). Evaluating a physiologically based pharmacokinetic model for predicting the pharmacokinetics of midazolam in Chinese after oral administration. Acta Pharmacol Sin 37(2): 276-284.
- Wang, Z. and E. C. Y. Chan (2022). Physiologically Based Pharmacokinetic Modelling-Guided Dose Management of Oral Anticoagulants when Initiating Paxlovid for COVID-19 Treatment. Clin Pharmacol Ther.
- Willmann, S., W. Schmitt, J. Keldenich, J. Lippert and J. B. Dressman (2004). A physiological model for the estimation of the fraction dose absorbed in humans. J Med Chem 47(16): 4022-4031.
- Yang, J., M. Jamei, K. R. Yeo, G. T. Tucker and A. Rostami-Hodjegan (2007). Prediction of intestinal first-pass drug metabolism. Curr Drug Metab 8(7): 676-684.

- Zane, N. R. and D. R. Thakker (2014). A physiologically based pharmacokinetic model for voriconazole disposition predicts intestinal first-pass metabolism in children. Clin Pharmacokinet 53(12): 1171-1182.
- Zanger, U. M. and M. Schwab (2013). Cytochrome P450 enzymes in drug metabolism: regulation of gene expression, enzyme activities, and impact of genetic variation. Pharmacol Ther 138(1): 103-141.